地震後航空機 SAR 画像のテクスチャ組み合わせによる 2016 年熊本地震の全壊建物の検出

DETECTION OF BUILDING DAMAGE DUE TO THE 2016 KUMAMOTO EARTHQUAKE USING TEXTURE COMBINATIONS OF SINGLE POST-EVENT AIRBORNE SAR IMAGE

19WM1315 BELLANIE YUNIKE ASTA LAPIAN　　指導教員 丸山　喜久
劉　ウェン

SYNOPSIS

Damage assessment is an essential issue in emergency response and recovery after the occurrence of natural disasters. In this regard, remote sensing is recognized as an effective tool for detecting and monitoring affected areas. In this study, we used full-polarimetric high-resolution Pi-SAR2-X images to detect the changes in Mashiki Town, which was severely affected by the 2016 Kumamoto Earthquake. This earthquake caused the collapse of many buildings, especially residential buildings. The backscatter model of a Japanese residential building is complicated due to its triangle roof shape. This study attempted to detect damage to triangle roof buildings using the four textures of the backscatter intensity from buildings' footprints and roofs. The affected buildings were identified by the high values of the heterogeneous texture and the low values of the homogeneous textures. As a result, the combination of two textures in the VV and HV polarizations was the most effective index to identify severely affected buildings.

1. Introduction

An Mw 6.2 earthquake hit the central part of Kumamoto prefecture, Japan, on 14 April 2016. The mainshock with Mw 7.3 then followed this earthquake occurred on 16 April, close to the first event. Due to the series of earthquakes, many damaged infrastructures were reported, including the collapse of Kumamoto Castle and the shinkansen's derailment. In addition, this earthquake caused significant damage to buildings. More than 160 thousand residential buildings were affected.

In order to grasp the damage situation quickly after a natural disaster strikes, remote sensing is recognized as a useful tool. Synthetic Aperture Radar (SAR) sensors can observe objects on the earth's surface without depending on sunlight and cloud conditions. The emergency observation of SAR images can be provided immediately soon after disasters. However, the lack of pre-event data limits their utility in damage detections. Therefore, it is vital to grasp the condition of damaged areas only from a post-event airborne SAR image. In addition to that, texture analysis in remote sensing images has become popular, especially for land-cover classification in recent years.

Thus, this study attempts to detect the most affected buildings using the texture characteristics obtained from a single airborne Pi-SAR image taken after the 2016 Kumamoto Earthquake. Four different textures were investigated for each building. Then the effective indices and their combinations were adopted to estimate building damages.

2. Study Area and Datasets

Central of Mashiki Town, near the epicenter of the mainshock, was selected as the study area in this study. We focused mainly on the area between the Akizu River and Prefectural Road 28, where most of the wooden buildings were severely affected by this earthquake.

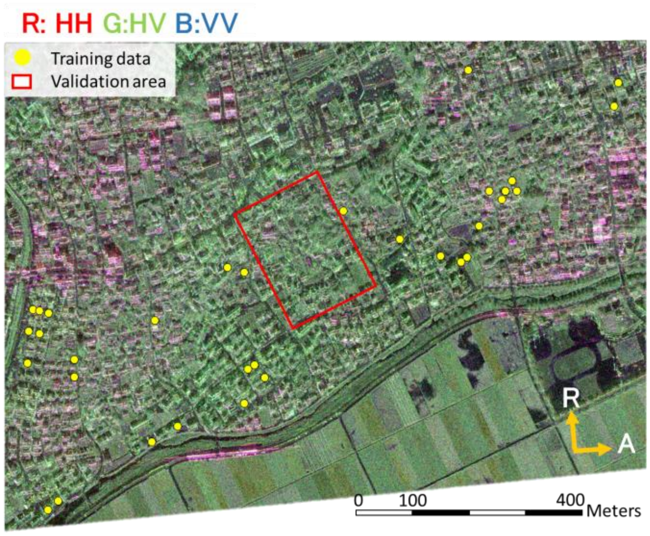

Figure 1 Color composite of Pi-SAR2-X polarization images in the target area of the Mashiki Town, including 42 training buildings (yellow dots) and the validation area (red frame)

In this study, we used an airborne Pi-SAR2-X image obtained by National Institute of Information and Communications Technology (NICT) on 17 April 2016, one day after the mainshock. The image was acquired in four polarizations (HH/HV/VH/VV) with an incidence angle of 37.6°. The azimuth angle was 83.0°clockwise from the north. **Figure 1** shows the color composite of the HH, HV and VV polarizations in the study area.

Three pre-processing steps were applied. First, the radiometric calibration was done to convert digital numbers into the backscattering coefficient (sigma naught σ^0), followed by geometric correction and speckle filter application.

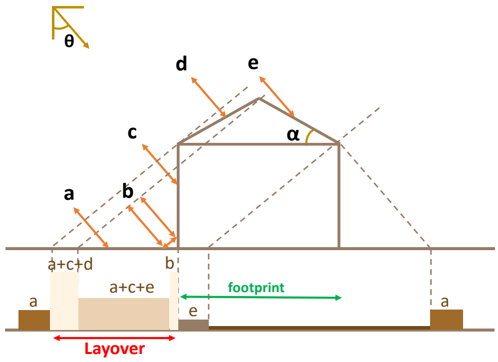

(a) $h < w \tan \theta$

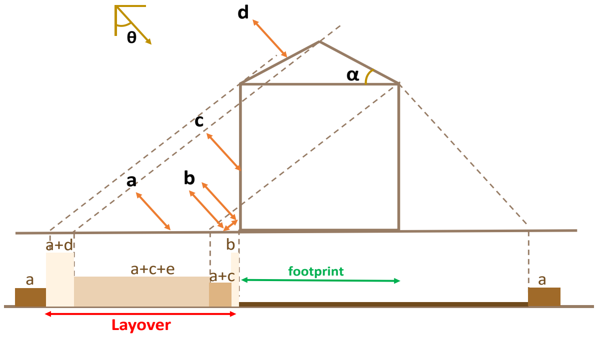

(b) $h > w \tan \theta$

Figure 2 Scattering models from different gable roof buildings

3. Building Extraction Regions

There are several previous studies regarding the building's backscatter model. Based on these studies[1),2)], the backscatter of a triangle-roof building can be divided into two categories depending on its height h and width w, as well as the relationship of the SAR incidence angle θ and the roof inclination α. In this study, all the buildings are in the type of $\alpha < \theta$. The two models with the different relationship of h and w are shown in **Fig. 2**. Most of the target buildings are following the model shown in **Fig. 2(a)**, where the backscatter from the roof (d and e) are overlapped on the layover from the wall, and the backscatter of roof opposite to the sensor (e) located inside of the footprint.

Several studies have extracted damaged buildings by focusing the backscatter characteristics in the layover regions. However, we found that this method is not very effective for the gable roof buildings. An example is shown in **Fig. 3**. Although the first floor of this building collapsed, based on the line profile, the strong shifted roof scattering was still confirmed in its original layover region. This is difficult to be distinguished from non-damaged buildings. Thus, in this study, we proposed new extraction regions for the texture analysis, pinpointing to the place where the buildings' essential backscatters were: the corner reflection near the footprint, and the roof reflection.

The extraction regions are created following the footprints and the layover positions. The footprints were traced from the GIS data published by the Geospatial Information of Authority (GSI). Then the layover is generated by moving the footprint according to the layover lengths L, calculated using building's height, SAR incidence angle θ, and radar sensors azimuth angle[3)]. In this study, the building's height is obtained from a Lidar data.

Following this, we took the boundary line between the footprint and the layover area as the footprint extraction line, while the end of the layover (nearest to the radar) as the roof extraction line. **Figure 4** shows the extraction regions on a building. Although most of the backscatter projected on these lines, there still are some backscatter drifted from these lines. Therefore, we expanded the extraction area with a 0.9-m (3 pixels) buffer. In addition, if the building has two sides or more facing the sensor direction, we investigated these sides individually in extraction, as sometimes damage only occurs on one side.

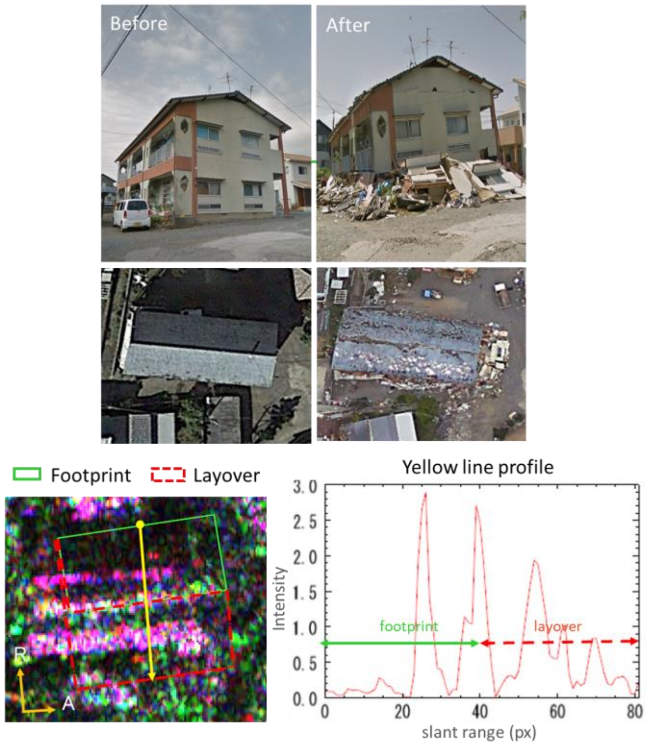

Fig. 3 Examination of a first-floor collapsed building by a profile line over the HH polarization image.

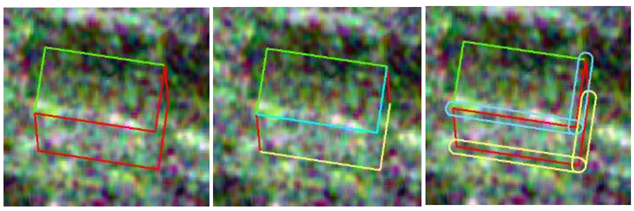

Traced layover (red) and footprint (green) | Extraction line: footprint (blue) layover (yellow) | Buffering zones and separating sides

Fig. 4 Generation of the footprint region (blue frame) and the roof region (yellow frame) for a gable roof building

4. Damage Detection Based on Texture Analysis

According to the previous research[4)], collapsed and survived buildings can be differentiated by their homogeneity and heterogeneity in the footprint. Thus, the second-order measure of the Gray Level Co-occurrence Matrix (GLCM)[5)] was used in this study. From the eight GLCM textures, *homogeneity* can measure the homogenous pixel values, whereas *contrast*, *dissimilarity*, and *variance* are suitable to measure heterogeneous values. Hence, we choose these four textures for damage detection.

A 9×9-pixel window was applied to the Pi-SAR2-X polarization images to calculate the GLCM textures in four directions (Horizontal: 0° or 90°, and Diagonal: 45° or 135°).

Both the single texture and the combination of all the textures were evaluated. To investigate the difference in the textures between damaged and non-damaged buildings, we selected 42 buildings as training data, including 18 collapsed buildings (D5) and 24 survived buildings (D0) as data in the target area.

(1) Single Texture Detection

Figure 5 shows the samples of one collapsed and one survived building. The GLCM textures are shown in **Fig. 5(b)-5(e),** where the red polygons are the extraction regions of collapsed (D5) building, and the yellow polygons are those of the survived (D0) building. Collapsed building showed lower value in *variance* (b), *contrast* (d) and *dissimilarity* (e), whereas higher values in *homogeneity* (b), within the footprint and roof extraction regions. The results for *variance*, *contrast* and *dissimilarity* showed the similar pattern because they belong to the same statistical texture group. The high *homogeneity* of the collapsed building may be caused by the reflection of debris. The corner reflection of debris located near the footprint region.

The best threshold values and the most valid textures were determined based on the kappa coefficient (κ), comparing with a truth data from the field study[6]. These results are shown in **Table 1**. The textures of HV polarization shows better results than other polarizations. Since the HV polarization is a cross-polarization, which is more sensitive to surface roughness. In addition, the textures in the footprint regions showed better results than those in the roof regions. It may be caused due to the errors in the roof extraction process with the wrong heights.

(2) Texture Combinations Detection

In order to improve the accuracy, we combined two textures for the detection. In choosing texture combinations, we used the 8 textures with the highest kappa coefficient shown in **Table 1**. Then they were evaluated using a multiple linear regression and a logistic regression. Both the regressions were used to understand the relationship of the textures[7]. **Figure 6** shows the comparison of kappa results from each texture combinations.

From the graph, the best three results are Linear Regression from the combination of BC, Logistic Regression from the combination of EH, and Logistic Regression from the combination of GH. Their kappa coefficients are 0.514, 0.533, and 0.483, respectively. Although using all texture combinations gave the best result (0.533 in Linear Regression and 0.539 in Logistic Regression), the required extraction time was significantly longer than using only two textures. Besides, the accuracy using all the texture only gave slightly improvement. Therefore, we chose the three combinations of two textures with highest κ for the damaged building detection.

With these three combinations, we can compare the results of three groups: two different kinds of texture and polarizations; two different textures in the same polarization; the same texture at different locations (footprint and roof).

5. Validation of Texture Combination Detection

Since the kappa coefficients using the combinations of two textures were higher than those using single texture, the texture combinations were applied to the test area. The test area included 48 buildings: 21 collapsed and 27 survived ones. Three combinations were considered for the evaluation based of the accuracy. All of the three combinations extracted 81.0% collapsed buildings.

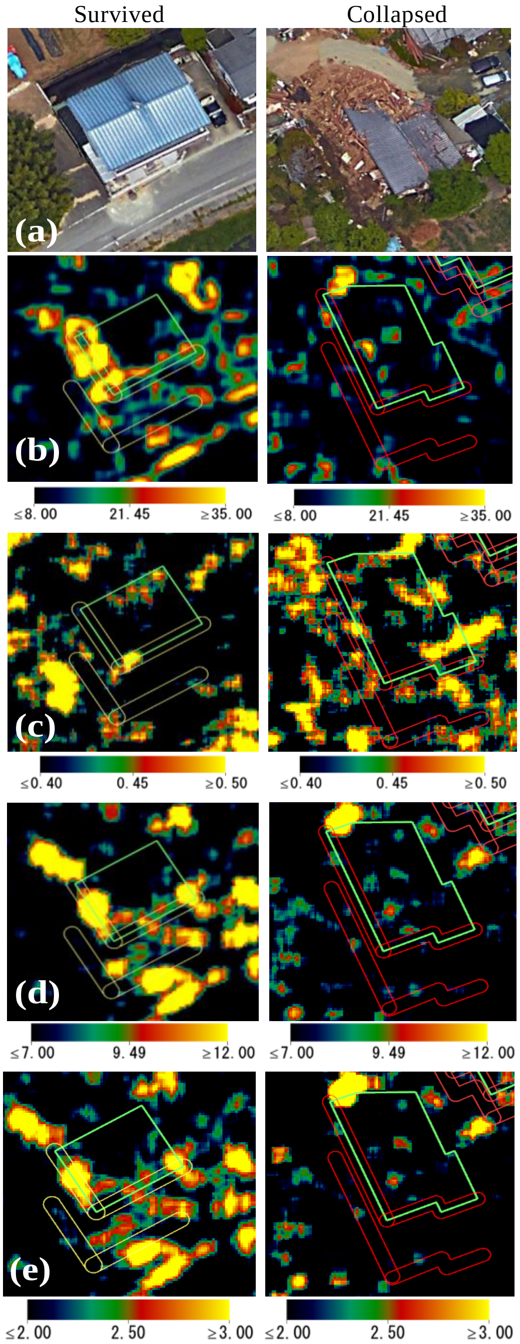

Fig. 5 Comparison of (a) aerial view and their GLCM textures HV polarization for a collapsed and a survived building: (b) variance, (c) homogeneity, (d) contrast and (e) dissimilarity.

Table 1 Accuracy assessment of best results in the single texture detection

			Threshold	κ	**Accuracy**
Variance	**HV**	F	11.876	0.372	0.667
	VV	F	11.772	0.413	0.548
Homogeneity	**HV**	F	0.391	0.462	0.738
		R	0.389	0.397	0.690
Contrast	**HV**	F	6.368	0.355	0.667
		R	5.319	0.446	0.738
Dissimilarity	**HV**	F	2.026	0.372	0.667
		R	1.849	0.364	0.690

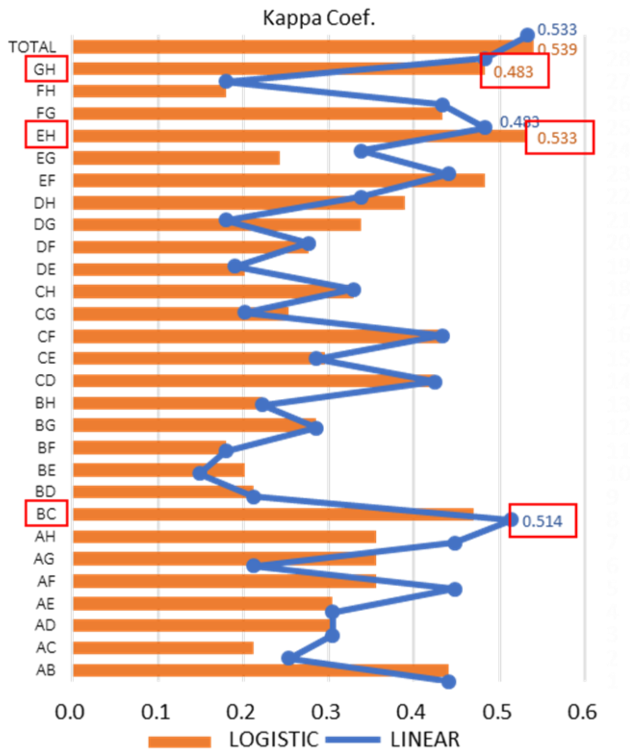

Fig. 6 Comparison of Kappa coefficients using different GLCM texture combinations, where A is Variance HV Footprint, B is Variance VV Footprint, C is Homogeneity HV Footprint, D is Homogeneity HV Roof, E is Contrast HV Footprint F is Contrast HV Roof, G is Dissimilarity HV Footprint, and H is Dissimilarity HV Roof, respectively. Three selected combinations for the validation are highlighted in red frames.

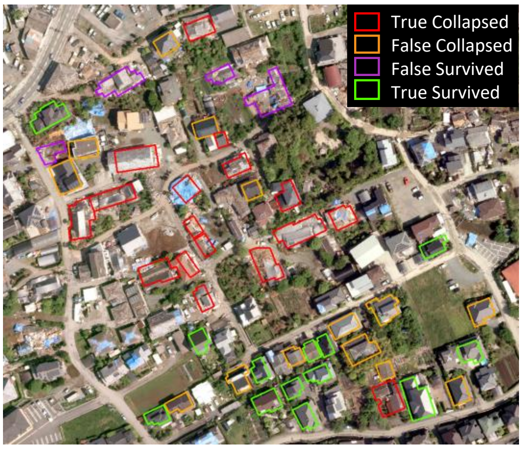

Fig. 7 Detection result (aerial view) from variance VV footprint & homogeneity HV footprint combination in validation area

Table 2 Confusion matrix of the classification using the combination of variance VV footprint & homogeneity HV footprint

		Truth data (Yamada et al.[6])			
		Collapsed	Survived	Total	U.A.
Prediction	Collapsed	17	14	31	54.8%
	Survived	4	13	17	76.5%
	Total	21	27	48	
	P.A.	81.0%	48.1%		
Overall Accuracy					0.625
Kappa					0.289
F					0.654

However, the combination of *variance* and *homogeneity* showed better precision for classifying collapsed buildings than the other combinations, which was 54.8% in user's accuracy (U. A.). This combination also obtained the best result in classifying the survived buildings with 48.1% in producer's accuracy (P. A.) and 76.5% in user's accuracy.

The result of the best combination is shown in **Fig. 7,** using the combination of *variance* in VV and *homogeneity* in HV polarization at the footprint area. The confusion matrix is shown in **Table 2.** This combination obtained overall accuracy of 62.5% in the test area. Although this accuracy was still low comparing with the previous studies, it showed the potential to overcome the limitation of damage detection using only one post-event SAR image. In addition, this combination was extracting the textures in only the buildings' footprints. Thus, height information of building was not necessary. Using only the buildings' footprints also could reduce the time in the extraction process.

6. Conclusions

The building damage extraction was attempted using the GLCM textures and their combinations from one Pi-SAR-X2 image acquired after the 2016 Kumamoto earthquake. In this study, the new extraction regions pinpointing the essential backscatter elements were adopted to investigate the textures of residential buildings. The combination of *variance* and *homogeneity* features showed the best capability to distinguish damaged and non-damage buildings. When those indicators were applied to a test area, 81% of collapsed buildings could be identified successfully.

REFERENCES

1) D. Brunner, G. Lemoine, L. Bruzzone, 2010. Earthquake damage assessment of buildings using VHR optical and SAR imagery. IEEE Trans. on Geosc. and R. Sensing, 48 (5), 2403–2420.
2) A. Thiele, E. Cadario, K. Schulz, U. Thoennessen and U. Soergel, 2007. Feature extraction of gable-roofed buildings from multi-aspect high-resolution InSAR data. IEEE International Geoscience and Remote Sensing Symposium, Barcelona, pp. 262-265.
3) F. Yamazaki, & Y. Iwasaki, W. Liu, T. Nonaka, & T. Sasagawa, 2013. Detection of damage to building side-walls in the 2011 Tohoku, Japan earthquake using high-resolution TerraSAR-X images. Proc SPIE. 8892. 12-. 10.1117/12.2029465.
4) L. Gong, C. Wang, F. Wu, J. Zhang, H. Zhang, & Q. Li, 2016. Earthquake-Induced Building Damage Detection with Post-Event Sub-Meter VHR TerraSAR-X Staring Spotlight Imagery. Remote Sensing, 8(11), 887. doi:10.3390/rs8110887
5) Haralick, R.M, Shanmugam, K., Dinstein, I., 1973. Textural features for the image classification, IEEE Trans. Systems, Man and Cybernetics, SMC-3:6, 610-621.
6) M. Yamada, J. Ohmura, & H. Goto, 2017. Wooden Building Damage Analysis in Mashiki Town for the 2016 Kumamoto Earthquakes on April 14 and 16. Earthquake Spectra. 33. 10.1193/090816EQS144M.
7) G.Tripepi, K. Jager, F. Dekker, & C. Zoccali, 2008. Linear and logistic regression analysis. Kidney international. 73. 806-10. 10.1038/sj.ki.5002787.